SUPPLEMENTAL MATERIAL

Viscoelastic Flows in Simple Liquids Generated by Vibrating Nanostructures

Matthew Pelton,[1] Debadi Chakraborty,[2] Edward Malachosky,[3] Philippe Guyot-Sionnest,[3] and John E. Sader[2,4]

[1]*Center for Nanoscale Materials, Argonne National Laboratory, Argonne, IL, 60439, U.S.A.*
[2]*Department of Mathematics and Statistics, The University of Melbourne, Victoria 3010, Australia*
[3]*James Franck Institute, University of Chicago, Chicago, IL, 60637, U.S.A.*
[4]*Kavli Nanoscience Institute and Department of Physics, California Institute of Technology, Pasadena, CA 91125, U.S.A.*

I. MATERIALS AND METHODS

A. Sample Preparation

Bipyramidal gold nanoparticles are synthesized in aqueous solution using a seed-mediated growth method. The synthesis follows the procedure described in Ref. 1. As well as bipyramidal gold nanoparticles, this synthesis also results in an irregular, spheroidal byproduct. The byproduct has a plasmon resonance around a wavelength of 550 nm, far away from the longitudinal plasmon resonance in the bipyramidal particles, which is centered around a wavelength of 760 nm. Optical measurements at the longitudinal-plasmon resonance frequency therefore probe only the bipyramids, and not the byproduct.

As synthesized, the particles are stabilized in aqueous solution with a large excess of cetyltrimethylammonium bromide (CTAB). This excess surfactant complicates transfer of the nanoparticles into different solvent mixtures, and can modify the viscosity and other physical properties of the solvent mixture. We therefore replace the CTAB with polystyrene sulphonic acid (PSS), a negatively charged polymer that coats the nanoparticles and stabilizes them without requiring excess polymer in solution.[1] In order to do this, the aqueous nanoparticle solution is first diluted to one fifth of its original volume and is then centrifuged at 5000 *g* for five minutes. The supernatant is then decanted, and the remaining pellet is suspended to the diluted volume in a 2:1 mixture of water and 0.1% PSS solution (by weight). The solution is left to stand for two hours, and is then again centrifuged at 5000 *g* for five minutes. The supernatant is decanted, and the pellet is resuspended in water to its original volume.

Small volumes of the resulting solutions of PSS-functionalized nanoparticles in water are added to larger volumes of water and glycerol to form the solutions that are measured optically. The quantities of water and glycerol to be mixed are measured by mass, with the aqueous nanoparticle solution

included in the water portion of the mixture. The solutions are stirred thoroughly to ensure that the mixtures are homogeneous. They are then transferred to optical cuvettes with a path length of 2 mm, taking care that no bubbles are introduced into the high-viscosity solutions in the process. The final concentration of the bipyramids in the solutions is such that the optical density in the 2-mm cuvettes at the longitudinal-plasmon resonance wavelength is between 0.1 and 0.2.

B. Transient-Absorption Measurements

Optical measurements are performed using a transient-absorption-spectroscopy system (Ultrafast Systems HELIOS). Measurement procedures follow those described in our previous publications.[2,3] Thermal artifacts are avoided by stirring the sample with a magnetic stir bar. Our previous measurements on high-viscosity samples involved mechanically translating the cuvette during measurements; we found, however, that this meant that the amount of pump light scattered into the detector varied over time, as bubbles in the solution and contaminants on the surfaces of the cuvette were translated through the pump beam. When the sample is stirred, by contrast, this scattering background is less variable over time, and can thus largely be subtracted from the measured signal by averaging eight spectra at negative time delays. We therefore limited our measurements to samples that could be stirred during the measurements, which meant that we could measure solutions up to a maximum mass fraction of 80% glycerol.

The temperature of the sample was monitored during measurements using a thermocouple immersed into the solution. The cuvette was sealed with the thermocouple in place, in order to prevent absorption of water from the environment into the water-glycerol mixtures.

C. Experimental Data Analysis

The background in the measured transient spectra due to scattered pump light is subtracted from all spectra, the measured signal is corrected for the fact that different probe wavelengths arrive at the focal spot at different times, and the time axis is adjusted so that the pump and probe overlap at time zero. The resulting spectrum at any given pump-probe time delay is then taken to be due to a shift in the longitudinal plasmon resonance frequency of the bipyramids and a broadening of the plasmon resonance line. Assuming that the extinction spectra with and without the pump laser are both Lorentzian functions, each transient spectrum thus has the following form:[2]

$$\Delta A(t) \propto \frac{1}{\Delta\omega^2 + \frac{1}{4}} - \frac{\gamma(t)}{[\Delta\Lambda(t) - \Delta\omega]^2 + \frac{1}{4}[\gamma(t)]^2}. \quad \text{(S1)}$$

This expression involves the following normalized frequencies: $\Delta\omega \equiv \omega_p - \Lambda_0/Z_0$, $\Delta\Lambda(t) \equiv \Lambda(t) - \Lambda_0/Z_0$, and $\gamma(t) \equiv Z(t)/Z_0$, where ω_p is the probe frequency; $\Lambda(t)$ and $Z(t)$ are the resonance frequency and linewidth, respectively, for a pump-probe delay t; and Λ_0 and Z_0 are the plasmon resonance frequency and linewidth in the absence of the pump pulse. These last two values are determined from the measured linear extinction spectrum of each sample. The remaining values are the fractional frequency shift and line broadening; these are determined for each time delay by least-squares fitting of the transient spectra for wavelengths between 650 and 830 nm. For measured spectra where there is a strong background of scattered pump light, wavelengths close to the pump wavelength are excluded from the fit. For spectra at certain time delays, the signal-to-noise ratio is not sufficient to allow for a good fit; these delays are omitted from the resulting time traces.

The time dependence of the peak shift, for pump-probe delays greater than 30 ps, consists of a damped oscillation on a decaying background. The oscillations are due to longitudinal acoustic vibrations of the bipyramids, and can be approximated as an exponentially damped sinusoid with frequency ω and decay time T_{tot}.[3,4,5,6] The background is due to the increased lattice temperature of the nanoparticles, and can be described over the measured time range as a decaying exponential with time constant τ_{cool}. We therefore fit the time-dependent peak shift using a least-squares method to the following function:

$$\Delta\Omega(t) = A_o \exp\left(-\frac{t}{T_{\text{tot}}}\right)\sin(\omega t + \phi) + A_1 \exp\left(-\frac{t}{\tau_{\text{cool}}}\right), \quad \text{(S2)}$$

where A_o, A_1, and ϕ are fitting parameters.[2,3] After the fit has been performed, the fitted second term can be subtracted from the data to obtain time traces that isolate the effects of acoustic oscillations, as in Figs. 1C and 2A.

For each water-glycerol mixture, measurements are made with pump-pulse energies of 120 nJ, 240 nJ, and 360 nJ, and values of T_{tot} and ω are determined for each of these pump energies. A linear least-squares fit is then performed for the dependence of T_{tot} and ω on pump power. The result of this fit is used to obtain values at zero power, which are the final values reported. The fitted decay time, T_{tot}, includes effects of the energy decay time, T, and the inhomogeneous dephasing time, T_{inh}. The inhomogeneous decay time depends on the distribution of nanoparticle dimensions. From analysis of

transmission-electron-microscope (TEM) images, we obtain the mean length, L_0, and standard deviation in length, σ_L, of the bipyramidal nanoparticles. Assuming that the lengths follow a normal distribution, the inhomogeneous damping time can be approximated as[3]

$$T_{\text{inh}} \approx \frac{\sqrt{2}L_o}{\omega\sigma_L}. \tag{S3}$$

For sufficiently weak inhomogeneous damping, the energy decay time can then be approximated according to[3]

$$\frac{1}{T} \approx \frac{1}{T_{\text{tot}}} - \frac{1}{T_{\text{inh}}}. \tag{S4}$$

A single adjustable parameter, Q_{int}, is also included when comparing measurements to theory. This intrinsic quality factor accounts for damping within the nanoparticles themselves, and has been determined from previous measurements of nanoparticles in low-viscosity fluids.[7] The total theoretical damping rate is then given by $1/Q = 1/Q_{\text{fluid}} + 1/Q_{\text{int}}$. The vibrational resonance frequency is $\omega_{\text{res}} = \omega/\sqrt{1 - 1/(4\,Q^2)}$.

II. ANALYTICAL MODELS

A. Newtonian Fluid

We assume that the oscillation amplitude of the particle is much smaller than any other geometric length scale, so that all nonlinear effects can be ignored.[8] This is the practical case and enables linearization of the equations of motion.[7,8] The required governing equation for the fluid motion is then the incompressible unsteady Stokes equation:

$$\boldsymbol{\nabla}\cdot\mathbf{v}=0, \qquad \rho\left(\frac{\partial\mathbf{v}}{\partial t}+\mathbf{v}\cdot\boldsymbol{\nabla}\mathbf{v}\right)=\boldsymbol{\nabla}\cdot\mathbf{T}, \tag{S5}$$

where $\mathbf{v}$ is the fluid velocity field and ρ is the fluid density. The Cauchy stress tensor is $\mathbf{T}=-p\mathbf{I}+\mathbf{S}$, where p is the fluid pressure, $\mathbf{I}$ is the identity tensor, and $\mathbf{S}$ is the deviatoric stress tensor. For an incompressible Newtonian fluid, $\mathbf{S}=2\mu\mathbf{D}$, where μ is the fluid shear viscosity and $\mathbf{D}=(\boldsymbol{\nabla}\mathbf{v}+\boldsymbol{\nabla}\mathbf{v}^{\mathrm{T}})/2$ is the rate-of-strain tensor.

The corresponding equation for the solid nanoparticle is Navier's equation:

$$\rho_s\frac{\partial^2\mathbf{u}}{\partial t^2}=\frac{E}{2(1+\sigma)}\left\{\boldsymbol{\nabla}^2\mathbf{u}+\frac{1}{(1-2\sigma)}\boldsymbol{\nabla}\left(\boldsymbol{\nabla}\cdot\mathbf{u}\right)\right\}, \tag{S6}$$

where $\mathbf{u}$ is the solid displacement field, ρ_s is the solid density, E the Young's modulus of the solid, and σ is the Poisson ratio of the solid.

Since the motion is oscillatory, all time-dependent variables, such as the solid displacement, fluid velocity and fluid pressure, are expressed in terms of the explicit time dependence $e^{-i\Omega t}$:

$$X(r,z,t)=\tilde{X}(r,z\,|\Omega)\,e^{-i\Omega t}, \tag{S7}$$

where i is the usual imaginary unit and X denotes any time-dependent quantity. For simplicity, we henceforth omit the superfluous '~' notation, noting that the above relation holds universally for harmonic oscillation.

At the interface between the fluid domain and the solid particle, the conditions of continuity of stress, velocity, and displacement are imposed. The no-slip boundary condition is enforced at the solid interface. This provides direct coupling between the Navier-Stokes equation for the fluid, equation (S5), and Navier's equation for the solid, equation (S6).

We simplify the calculations by approximating the nanoparticles as axisymmetric. A bipyramid is thus approximated as a pair of truncated cones, as illustrated in Fig. S1. Each half of the particle along its symmetry axis is a cone with a base diameter of $R_{\max}$ and a height of $L_T/2$, truncated to a height of $L/2$, so that the total length of the particle is L.

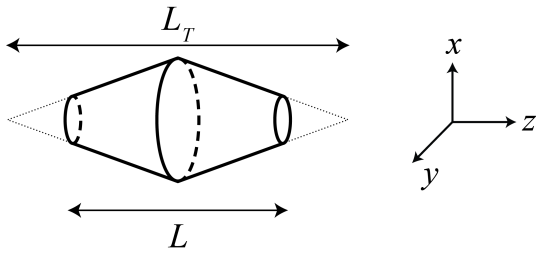

Figure S1: Schematic of the bipyramid particle geometry used for calculations. The origin is at the center of the particle.

An analytical solution to this problem can be obtained by assuming that the length of the particle greatly exceeds both the viscous penetration depth and the particle radius.[7] This allows for approximation of the hydrodynamic load at any axial position along the particle by that due to a local shear flow; pressure does not affect the flow in this limit. We then obtain the following normalized, complex eigenfrequency for the vibration:[7]

$$\overline{\Omega}^2 \equiv \left(\frac{L^2\rho_s}{E}\right)\Omega^2 \frac{\int_0^{\frac{1}{2}} R^2(z)\left(u'(z)\right)^2 dz}{\int_0^{\frac{1}{2}}\left(R^2(z) + (1+i)\frac{\rho}{\rho_s}R_{\max}\,R(z)\sqrt{\frac{1}{\beta(\Omega)}}\,K^*\right)u^2(z)dz}, \qquad \text{(S8)}$$

where Ω is the complex eigenfrequency, $R(z)$ is the position-dependent radius of the particle, z is the distance along the particle, normalized by L, and $K^* = K_1\left(-i\sqrt{2i\beta(\Omega)}\,R(z)/R_{\max}\right)/K_0\left(-i\sqrt{2i\beta(\Omega)}\,R(z)/R_{\max}\right)$. In this expression, the Reynolds number is

$$\beta(\Omega) = \frac{\rho\Omega R_{\max}^2}{2\mu}. \qquad \text{(S9)}$$

The integrals in equation (S8) must be evaluated numerically. The equation then becomes a transcendental equation for the complex eigenfrequency, Ω. The resonant frequency, ω_{res}, and quality factor, Q_{fluid}, of the nanoparticle vibrations can be determined from this eigenfrequency:

$$\omega_{\mathrm{res}} = \sqrt{\Omega_{\mathrm{r}}^2 + \Omega_{\mathrm{i}}^2}\ , \tag{S10}$$

and

$$Q_{\mathrm{fluid}} = -\frac{\omega_{\mathrm{res}}}{2\Omega_{\mathrm{i}}}\ , \tag{S11}$$

where Ω_{r} and Ω_{i} are the real and imaginary components of Ω, respectively.

B. Linear Maxwell Fluid

The model developed above can readily be generalized to the case of a linear Maxwell fluid. In this case, the deviatoric stress tensor is given by[9]

$$\mathbf{S} + \lambda\frac{\partial \mathbf{S}}{\partial \mathrm{t}} = 2\mu\mathbf{D}, \tag{S12}$$

where λ is the shear relaxation time of the fluid. Applying the harmonic time dependence of equation (S7), equation (S11) becomes $\mathbf{S} - i\Omega\lambda\mathbf{S} = 2\mu\mathbf{D}$, which has the explicit solution

$$\mathbf{S} = \frac{2\mu}{1 - i\Omega\lambda}\mathbf{D}. \tag{S13}$$

The solution for a Maxwell fluid can thus be rigorously obtained from that of a Newtonian fluid, under the substitution

$$\mu \rightarrow \frac{\mu}{1 - i\Omega\lambda}. \tag{S14}$$

In particular, making this substitution in equation (S9) enables calculation of the dynamic response of a nanoparticle immersed in a linear Maxwell fluid, from equation (S8).

III. FINITE-ELEMENT CALCULATIONS

Finite-element calculations solve the same eigenvalue problem, equations (S5) - (S7), as the analytical model described above, subject to the same boundary conditions. In particular, we assume that the oscillation amplitude of the nanoparticles is small, and we apply the no-slip boundary condition at the solid-liquid interface. Numerical solution of the equations, however, makes it possible to remove the approximation of long, slender nanoparticles, and consider cases where the nanoparticle length is arbitrary relative to its diameter or to the viscous penetration depth in the fluid.

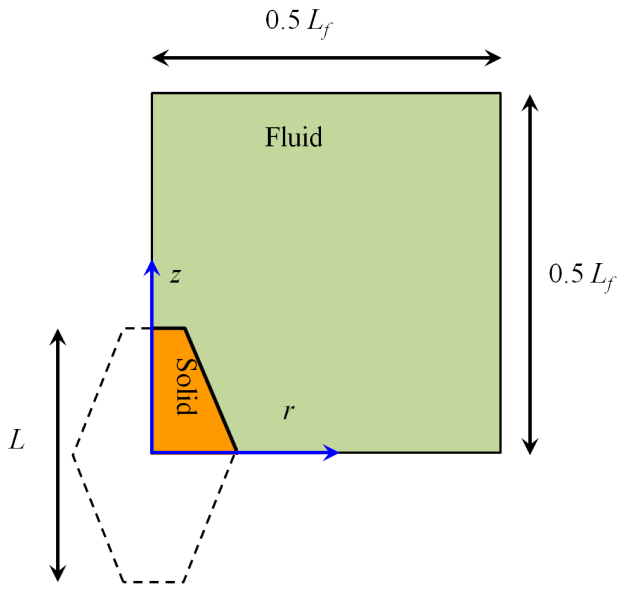

Figure S2: Schematic of a bipyramidal nanoparticle immersed in a fluid, showing the computational domain and particle dimensions. The line along the z-direction through the major axis of the particle is the axis of symmetry. The fluid region is green and the solid region is gold. The dashed region is not part of the computational domain, and is shown only to illustrate the particle shape.

In the finite-element calculations, we again assume cylindrical symmetry, approximating the bipyramidal nanoparticle as a pair of truncated cones, as illustrated in Fig. S1. This symmetry makes it possible to reduce the computational domain to the r-z plane for $z \geq 0$, where the z-axis is along the symmetry axis of the particle, r is the radial direction, and the origin is at the center of the particle. The fluid domain is taken to extend a distance $L_f/2$ in both the r and z-directions from the center of the particle, as illustrated in Fig. S2, and the condition of zero fluid pressure is applied at these boundaries. This allows for flow into and out of the boundaries, and thus presents a weaker boundary condition than a no-penetration or no-slip condition, lessening the effect of the finite computational domain.

The resulting coupled system of equations is implemented in the commercial finite-element software COMSOL Multiphysics, using its damped eigenfrequency solver. The effects of the computational domain are assessed by varying the size of the fluid domain while keeping the nanoparticle dimensions fixed. This shows that $L_{\mathrm{f}} \geq 6\, L_{\mathrm{T}}$ ensures calculated quality factors and resonant frequencies are independent of domain size to within 0.1%; we therefore use $L_{\mathrm{f}} = 10\, L_{\mathrm{T}}$ in all reported calculations. We use a high-density mesh at the liquid-solid interface, to capture effects due to the viscous boundary layer, and verify that a mesh with 23,625 elements provides results that are independent of mesh size to within 0.1%. We also verify that the finite-element results agree quantitatively with the analytical theory for particles with aspect ratio $L_{\mathrm{T}}/(2R_{\mathrm{max}}) \geq 100$.

IV. MATERIAL PROPERTIES

A. Gold Nanoparticles

For all calculations, the gold nanoparticles are taken to have bulk material properties,[6] specifically, a density of 19,320 kg/m^3 and a Poisson's ratio of 0.44.[10] Young's modulus is not required, because the data is normalized by the measured resonant frequencies.

B. Glycerol-Water Mixtures

Standard low-frequency shear viscosities for the water-glycerol mixtures are calculated according to the empirical formula in Ref. 11. The temperatures of the solutions measured during the optical measurements are substituted into this formula, together with the mass fraction of glycerol in the mixture.

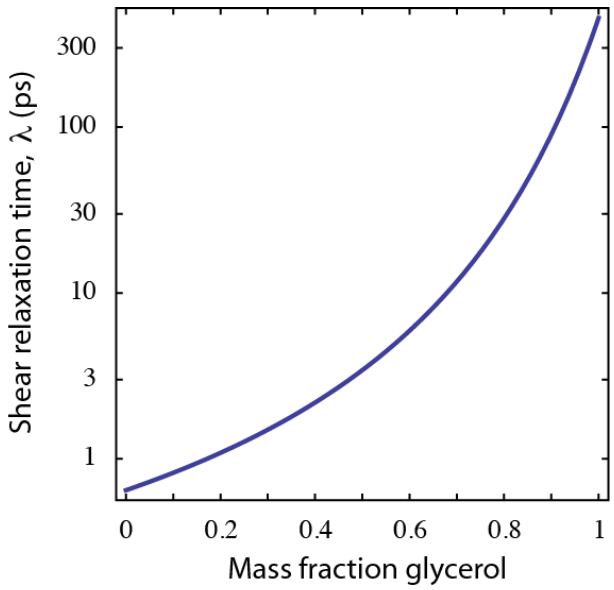

Figure S3: Shear relaxation time, λ, as a function of mass fraction of glycerol, for glycerol/water mixtures at 25°C.

Calculations for a linear Maxwell fluid use tabulated values for the relaxation time, λ, previously obtained from ultrasonic measurements.[12] The shear relaxation time is given by the ratio of the low-frequency shear viscosity, μ, to the high-frequency shear modulus, G_∞:

$$\lambda = \frac{\mu}{G_\infty} . \tag{S15}$$

Slie *et al.* showed that G_∞ is weakly dependent on the concentration of glycerol and temperature.[12] Based on this measured data, and extrapolation to 100% water, they derived empirical relations for the infinite frequency shear modulus G_∞ as a function of water concentration and temperature (see Table II of Ref. 12). Since the fit coefficients vary linearly with water concentration and temperature, it is a simple matter to derive a general fit function that includes both effects. Performing linear regression on these fit parameters then gives

$$G_\infty = (2.67867 - 0.99291\, c) - (0.02762 - 0.01544\, c)\, T \qquad \text{[GPa]}, \qquad \text{(S16)}$$

where c is the mole fraction of water and T is the temperature in °C. The resulting dependence of λ on the mass fraction of glycerol, for water-glycerol mixtures at 25°C, is given in Fig. S3. The limiting values for the shear relaxation time predicted by equation (S16) are in good agreement with independent reports for water and pure glycerol.[13,14]

V. TESTS OF MODEL ASSUMPTIONS

A. Effect of Fluid Compressibility

The analytical models described above implicitly assume that flow is driven only by shear, since they are derived for a slender particle undergoing extensional oscillations. These analytical models therefore have zero pressure variations, and give identical predictions for both compressible and incompressible Newtonian fluids. However, they show good agreement with full finite-element simulations for incompressible flow,[7] especially for slender particles. The finite-element simulations account for the full three-dimensional geometry of the particles and thus accurately capture pressure effects at the particle ends. This agreement between the analytical models and finite-element simulations indicates that pressure variations do not exert a strong effect on the fluid-structure interaction. Since fluid compressibility affects flow behaviour and energy dissipation through pressure variations only, fluid compressibility is expected to exert a secondary effect.

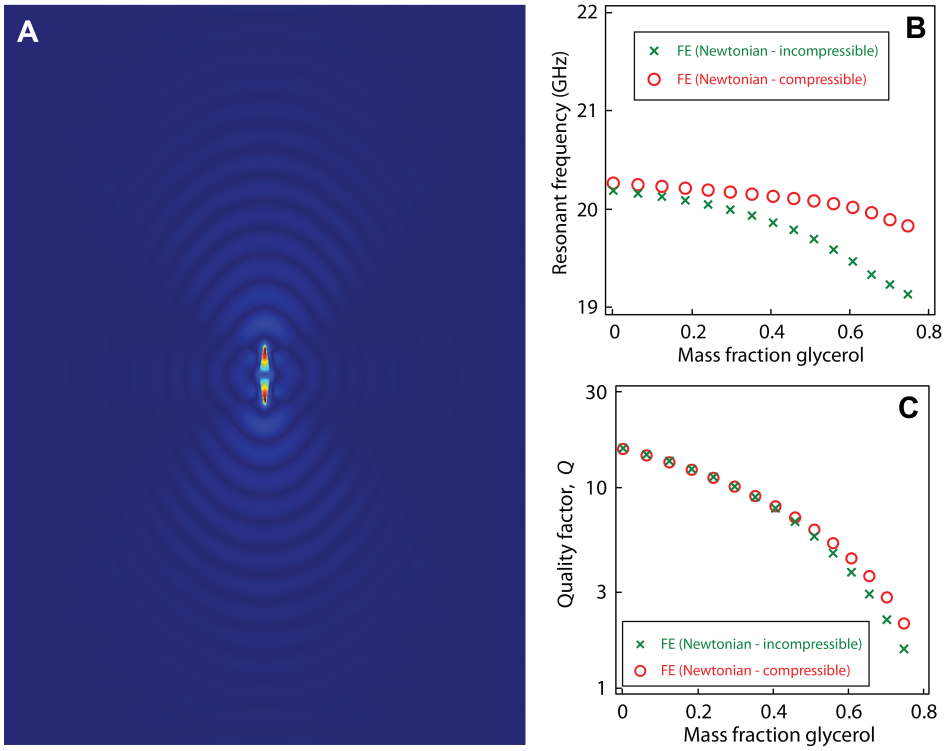

Figure S4: Effect of fluid compressibility. **A.** Velocity field in a vibrating bipyramidal gold nanoparticle and in surrounding pure water, showing sound wave propagation away from the particle. **B & C.** Calculated resonant frequency and quality factor for vibrations of bipyramidal gold nanoparticles in water-glycerol mixtures. Results are shown for an incompressible Newtonian fluid, assuming an intrinsic quality factor $Q_{\mathrm{int}} = 50$ (7), and for a compressible Newtonian fluid, assuming $Q_{\mathrm{int}} = 90$.

We verified this explicitly by performing finite-element simulations that treat the liquid surrounding the nanoparticle as a compressible Newtonian fluid. Using the true particle geometry in these calculations rigorously accounts for pressure effects at the particle ends, and thus the fluid compressibility. Figure S4(A) shows the velocity field in the particle and the fluid for a bipyramid vibrating in water. As expected, sound waves are observed to radiate mainly from the particle ends, demonstrating that this is indeed predominantly a shear-driven flow. Compressibility modifies the effect of fluid loading especially at high viscosity, and a monotonic decrease in both the resonant frequency and quality factor with increasing glycerol is observed; see Figs. S4(B) and S4(C). Fluid compressibility is therefore unable to account for the experimental observations.

B. Effect of Slip at the Solid-Liquid Interface

The models presented above can be generalized by replacing the no-slip boundary condition with a slip boundary condition. We implement the standard Navier slip condition:

$$u_{\text{slip}} = \eta\, \mathbf{n} \cdot \nabla \mathbf{v} \cdot \mathbf{t}\,, \tag{S17}$$

where η is a molecular length scale of the fluid, commonly referred to as a slip length, **n** is the unit normal vector to the surface, **v** is the velocity field, and **t** is the unit tangent vector to the surface.

Figure S5 shows results of the analytical model that allows for slip at the solid-liquid interface, assuming a Newtonian fluid; similar conclusions are obtained using finite-element analysis. Realistic values of the normalized molecular scale, or Knudsen number, $\text{Kn} \equiv \eta/R_{\text{max}}$, are less than 10^{-3}. For these values, the calculated resonant frequencies and quality factors are nearly identical to those obtained using the no-slip boundary condition. Assuming high values of Kn leads to unrealistically low damping for low-viscosity fluids. Including slip in the calculations thus does not capture the observed experimental trend.

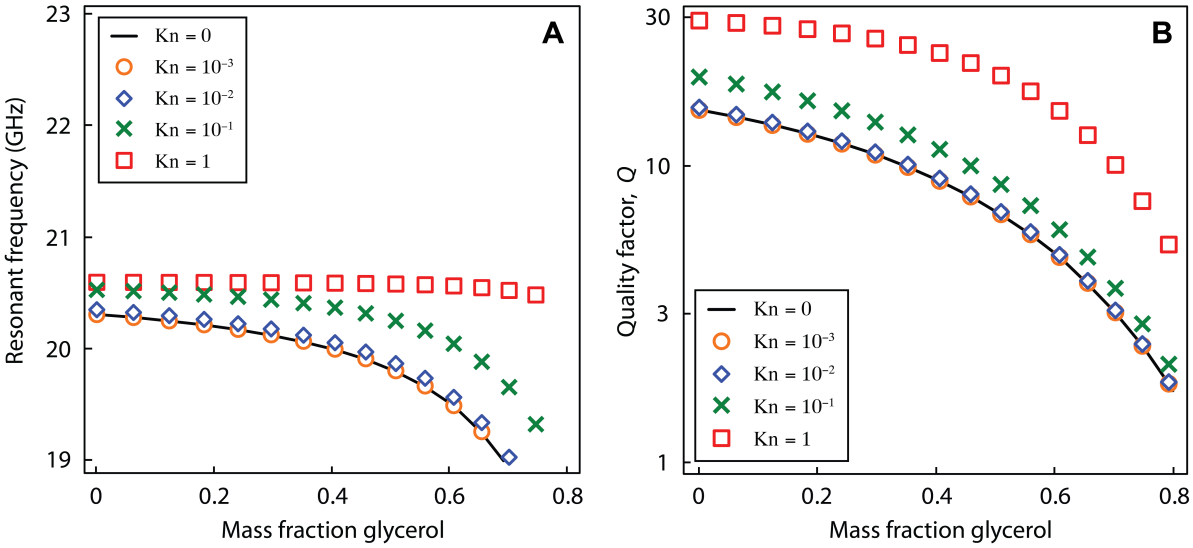

Figure S5: Effect of slip on the calculated **A.** resonant frequencies and **B.** quality factors for bipyramidal gold nanoparticles in water-glycerol mixtures, as a function of the mass fraction of glycerol. Results are shown for Newtonian fluids with different Knudsen numbers, Kn, and assume an intrinsic quality factor, $Q_{\text{int}} = 35$.

VI. MAXIMUM POTENTIAL-ENERGY DENSITY IN SOLID AND FLUID DOMAINS

A. Solid Particle

The potential energy per unit volume, E_{solid}, stored in a linearly elastic solid is

$$E_{\text{solid}} = \frac{1}{2}\mathbf{T} : \mathbf{e}\,, \tag{S18}$$

where $\mathbf{T}$ is the stress tensor and $\mathbf{e}$ is the strain tensor. Integrating equation (S18) over the entire volume of the solid gives the total potential energy.

Since the motion is harmonic, we apply the ansatz in equation (S7) and consider the real parts of the complex-valued stress and strain tensors:

$$\mathbf{T} = \text{Re}\{\tilde{\mathbf{T}}\, e^{-i\omega t}\}\,, \quad \mathbf{e} = \text{Re}\{\tilde{\mathbf{e}}\, e^{-i\omega t}\}\,. \tag{S19}$$

Choice of the real part merely sets the phase reference in the oscillatory motion, and does not affect the final result for the energy stored.

Retaining the "~" for clarity here, we obtain the required expression for the maximum energy stored in the solid in terms of the complex stress and strain tensors:

$$\max\{E_{\text{solid}}\} = \frac{1}{4}\left(\text{Re}\{\tilde{\mathbf{T}} : \tilde{\mathbf{e}}^{*}\} + \left|\tilde{\mathbf{T}} : \tilde{\mathbf{e}}\right|\right), \tag{S20}$$

where * indicates the complex conjugate.

Equation (S20) applies to any linearly elastic solid, regardless of the constitutive equation. It is used to calculate the maximum energy density stored in the solid particle.

B. Surrounding Fluid

The constitutive equation for a linear Maxwell fluid is given in equation (S12):

$$\mathbf{S} + \lambda\frac{\partial \mathbf{S}}{\partial \mathrm{t}} = 2\mu\mathbf{D}, \tag{S21}$$

where the total stress is $\mathbf{T} = -p\mathbf{I} + \mathbf{S}$, p is the pressure, and $\mathbf{S}$ is the deviatoric stress tensor. The rate of work done in deforming a material element of the fluid is

$$W = \mathbf{T} : \mathbf{D} = \mathbf{S} : \mathbf{D}\,, \tag{S22}$$

where we have assumed that the fluid is incompressible.

Substituting equation (S21) into equation (S22) gives

$$W = \frac{1}{2\mu}\mathbf{S}:\mathbf{S} + \frac{\lambda}{4\mu}\frac{\partial}{\partial t}(\mathbf{S}:\mathbf{S}). \tag{S23}$$

The second term on the right hand side of equation (S23) does not contribute to the energy dissipated per cycle and defines the rate-of-change for the energy density stored in the fluid:

$$E_{\text{fluid}} = \frac{\lambda}{4\mu}\mathbf{S}:\mathbf{S}. \tag{S24}$$

Equation (S24) can also be obtained from equation (S18) by noting that a linear Maxwell fluid corresponds to a spring connected to a damper in series. Substituting the spring contribution to the total rate-of-strain into equation (S18) immediately gives equation (S24).

Finally, we substitute the time ansatz for harmonic motion,

$$\mathbf{T} = \text{Re}\{\tilde{\mathbf{T}}\, e^{-i\omega t}\}, \quad \mathbf{S} = \text{Re}\{\tilde{\mathbf{S}}\, e^{-i\omega t}\}, \quad p = \text{Re}\{\tilde{p}\, e^{-i\omega t}\}, \tag{S25}$$

into equation (S24), to obtain the required result for the maximum energy density stored in the fluid:

$$\max\{E_{\text{fluid}}\} = \frac{\lambda}{8\mu}\left(\tilde{\mathbf{S}}:\tilde{\mathbf{S}}^{*} + \left|\tilde{\mathbf{S}}:\tilde{\mathbf{S}}\right|\right) = \frac{\lambda}{8\mu}\left(\tilde{\mathbf{T}}:\tilde{\mathbf{T}}^{*} - 3|\tilde{p}|^{2} + \left|\tilde{\mathbf{T}}:\tilde{\mathbf{T}} - 3\tilde{p}^{2}\right|\right). \tag{S26}$$

This equation is used to calculate the maximum energy density stored in the fluid.

VII. EFFECT OF MOLECULAR ORDERING OF LIQUID AND PSS LAYER

The principal experimental observation of this study is that the resonant frequency of the nanoparticles increases with increasing glycerol concentration; this feature is not predicted using Newtonian theory (see Fig 2C). Here, we show that molecular ordering of the liquid at the solid-liquid interface and/or a change in conformation of the PSS layer surrounding the nanoparticles cannot be responsible for this observation.

A. Vacuum Frequency

We first calculate the resonant frequency of the particles in the absence of liquid, *i.e.,* in vacuum. This value is then used as a reference for discussion. Since Newtonian theory holds for water,[2] the vacuum frequency of the particle can be calculated from the measurement in water. The principal equation for the Newtonian theory is[7]

$$\left(\frac{L^2\rho_s}{E}\right)\omega^2 = \frac{\int_0^{\frac{1}{2}} R^2(z)\left(u'(z)\right)^2 dz}{\int_0^{\frac{1}{2}}\left(R^2(z) + (1+i)\frac{\rho}{\rho_s}R_{\max}R(z)\sqrt{\frac{1}{\beta(\omega)}}\,K^*(\omega,z)\right)u^2(z)dz}\,, \qquad \text{(S27)}$$

where ω is the complex eigenfrequency, L is the particle length, ρ_s is the particle density, E is the Young's modulus of the particle, ρ is the fluid density, μ is the fluid shear viscosity, $u(z)$ is the position-dependent axial displacement of the particle, $R(z)$ is the position-dependent radius of the particle, $R_{\max}$ is the maximum particle radius, $u(z)$ is the position-dependent displacement of the particle in the z-direction, $K^*(\omega,z) = K_1\left(-i\sqrt{2i\beta(\omega)}\,R(z)/R_{\max}\right)/K_0\left(-i\sqrt{2i\beta(\omega)}\,R(z)/R_{\max}\right)$, K_0 and K_1 are modified Bessel functions of the third kind, and $\beta(\omega) = \rho\omega R_{\max}^2/(2\mu)$. Integration in Eq. (S27) is over one half of the bipyramid particle length, by symmetry.

The resonant frequency in fluid, ω_{fluid}, is related to the complex eigenfrequency ω by

$$\omega_{\text{fluid}} = \sqrt{\omega_{\text{i}}^2 + \omega_{\text{r}}^2}\,. \qquad \text{(S28)}$$

The resonant frequency in vacuum is obtained by setting the fluid density to zero in Eq. (S27). Calculations using Eqs. (S27) and (S28) display excellent agreement with full FE simulations of the fluid-structure problem.

Substituting the measured value for the resonant frequency of the nanoparticles in pure water,

$$f_{\text{water}} = 20.3\ \text{GHz}\,, \tag{S29}$$

into Eqs. (S27) and (S28), and solving for the vacuum frequency, gives the required result for the resonant frequency in vacuum:

$$f_{\text{vac}} = 20.6\ \text{GHz}\,. \tag{S30}$$

B. Effect of Increasing Glycerol Concentration

Increasing glycerol concentration above 40% is experimentally observed to strongly increase the measured resonant frequency. (See Fig. 2C in the main text.) Strikingly, the vacuum frequency of $f_{\text{vac}} = 20.6\ \text{GHz}$, calculated above, is significantly smaller than the measurement in an 80% glycerol/water mixture:

$$f_{80\%\ \text{glycerol}} = 22.3\ \text{GHz}\,. \tag{S31}$$

This is to be compared to the 1.5% reduction in frequency from vacuum to water.

This strong increase in resonant frequency with increasing glycerol concentration is not predicted using Newtonian theory and immediately establishes that presence of the surrounding glycerol mixture stiffens the particle.

C. Effect of Interfacial Liquid and PSS Layers

We now examine the possible role of interfacial molecular ordering of the liquid and conformational changes in the PSS layer surrounding the particle surface. Specifically, we explore the possibility that these effects alone could account for the large increase in resonant frequency from vacuum to 80% glycerol. Such a large increase in resonant frequency would require an interfacial liquid layer and/or PSS layer that strongly increases the effective rigidity of the metal nanoparticle.

If we assume these layers have identical elastic properties to gold, but with the density of water, then the layers would need to be approximately 2 nm thick to account for the frequency increase described above. This thickness value is obtained by noting that, under such conditions, the potential energy increases linearly with the cross sectional area, whereas the kinetic energy is relatively unchanged (due to the difference in the density of gold and water). Even so, the existence of either liquid or PSS layers with the elastic properties of a metal is clearly unphysical; this thickness estimate is therefore a lower bound. Decreasing the rigidity of such layers from the values of gold would increase the required layer thickness. Indeed, realistic elastic properties of these layers would require

that they be dramatically larger than the particle diameter in order to account for the observed increased in frequency.

However, the thickness of the PSS layer is limited to a few nm by the size of the PSS molecules, as has been directly observed in TEM images. This immediately eliminates the possibility that the PSS layer is responsible for the observed increase in frequency. Similarly, long-range molecular ordering of the liquid over hundreds or thousands of nanometers from the particle surface is also unphysical; this rules out the possibility that interfacial liquid effects are responsible for the observations.

REFERENCES

[1] M. Liu and P. Guyot-Sionnest, J. Phys. Chem. B **109**, 22192 (2005).

[2] M. Pelton, J. E. Sader, J. Burgin, M. Liu, M., P. Guyot-Sionnest, and D. Gosztola, Nat. Nano. **4**, 492 (2009).

[3] M. Pelton, Y. Wang, D. Gosztola, and J. E. Sader, J. Phys. Chem. C **115**, 23732 (2011).

[4] C. Voisin, N. Del Fatti, D. Christofilos, and F. Vallée, J. Phys. Chem. B **105**, 2264 (2001).

[5] G. V. Hartland, Annu. Rev. Phys. Chem. **57**, 403 (2006).

[6] G. V. Hartland, Chem. Rev. **111**, 3858 (2011).

[7] D. Chakraborty, E. van Leeuwen, M. Pelton, and J. E. Sader, J. Phys. Chem. C **117**, 8536 (2013).

[8] J. E. Sader, J. Appl. Phys. **84**, 64 (1998).

[9] E. R. Schowalter, *Mechanics of Non-Newtonian Fluids* (Permagon Press, Oxford, 1978).

[10] M. Hu *et al.,* J. Am. Chem. Soc. **125**, 14925 (2003).

[11] N.-S. Cheng, Ind. Eng. Chem. Res. **47**, 3285 (2008).

[12] W. M. Slie, A. R. Donfor, and T. A. Litovitz, J. Chem. Phys. **44**, 3712 (1966).

[13] R. Piccirelli and T. A. Litovitz, J. Acous. Soc. Am. **29**, 1009 (1957).

[14] G. D'Arrigo, J. Chem. Phys. **75**, 921 (1981).